Citation: Molecular Therapy—Nucleic Acids (2016) 5, e318; doi:10.1038/mtna.2016.28
Official journal of the American Society of Gene & Cell Therapy
www.nature.com/mtna

A Tumor-specific MicroRNA Recognition System Facilitates the Accurate Targeting to Tumor Cells by Magnetic Nanoparticles

Yingting Yu[1], Yi Yao[1], Hao Yan[2], Rui Wang[1], Zhenming Zhang[1], Xiaodan Sun[2], Lingyun Zhao[2], Xiang Ao[1], Zhen Xie[3,4] and Qiong Wu[1]

Targeted therapy for cancer is a research area of great interest, and magnetic nanoparticles (MNPs) show great potential as targeted carriers for therapeutics. One important class of cancer biomarkers is microRNAs (miRNAs), which play a significant role in tumor initiation and progression. In this study, a cascade recognition system containing multiple plasmids, including a Tet activator, a lacI repressor gene driven by the TetOn promoter, and a reporter gene repressed by the lacI repressor and influenced by multiple endogenous miRNAs, was used to recognize cells that display miRNA signals that are characteristic of cancer. For this purpose, three types of signal miRNAs with high proliferation and metastasis abilities were chosen (miR-21, miR-145, and miR-9). The response of this system to the human breast cancer MCF-7 cell line was 3.2-fold higher than that to the human breast epithelial HBL100 cell line and almost 7.5-fold higher than that to human embryonic kidney HEK293T cells. In combination with polyethyleneimine-modified MNPs, this recognition system targeted the tumor location *in situ* in an animal model, and an ~42% repression of tumor growth was achieved. Our study provides a new combination of magnetic nanocarrier and gene therapy based on miRNAs that are active *in vivo*, which has potential for use in future cancer therapies.

Molecular Therapy—Nucleic Acids (2016) **5**, e318; doi:10.1038/mtna.2016.28; published online 3 May 2016
Subject Category: siRNAs, shRNAs and miRNAs nanoparticles

Introduction

Cancer is one of the largest threats to public health worldwide and is responsible for approximately one-quarter of all deaths in the United States.[1] Convenient and accurate methods for cancer treatment and diagnosis are urgently needed, in addition to traditional surgery, chemotherapy, and radiation therapy, which may have serious side effects.[2,3] Among the many potential approaches for cancer treatment, gene therapy based on a biocompatible nanomaterial carrier holds great promise.[4,5] These approaches show better efficiency and selectivity than do other novel therapies and, as such, have many favorable prospects.[6,7]

As recently reported, the abnormal expression of miRNAs is closely related to various types of cancers, such as breast cancer,[8] lung cancer[9], and colon cancer,[10] because of the significant role of microRNAs (miRNAs) in the posttranscriptional regulation of genes.[11] To some extent, this expression reflects the developmental lineage and differentiation state of the tumors.[12] For example, miR-21 is upregulated in many cancers,[13,14] and its overexpression in an *in vivo* model induces the generation of tumors, such as pre-B-cell lymphoma.[15] Thus, miRNAs might be used as genomic medicine targets or biomarkers to identify cancer cells in gene therapy for cancer.[16–19]

Researchers have already attempted to apply cancer treatments based on tissue/cancer-specific miRNAs.[20–24] For instance, a multiinput RNAi-based logic circuit containing several types of miRNA sensors can differentiate HeLa cancer cells from non-HeLa cells by endogenous specific miRNA matching.[24] Such achievements offer a choice for gene therapy, with tumor cell specificity guaranteed by cancer-specific miRNAs. miRNAs pair with target mRNAs containing the corresponding miRNA pairing site downstream of the gene, thereby leading to expression silencing;[11] thus, tissue/cancer-specific miRNA may selectively inhibit designed artificial gene elements. These results suggest that miRNAs may be used as biomarkers and have great potential in cancer therapy.

In addition to specific tumor cell selection realized by an artificial gene element, suitable tools for delivering these elements are also needed. Various biocompatible nanomaterials have been applied as drug and gene carriers,[25] such as chitosan,[26] polyethylene glycol (PEG)[27], and liposomes.[28] Nanoparticles with diameters of less than 100 nm, in addition to having good biocompatibility and nontoxicity, can pass through abnormal blood vessels in tumor sites that have a loose vascular membrane morphology (the so-called enhanced permeability and retention effect)[29] and display clearance behavior *in vivo*,[30] thus making them suitable for tumor targeting as delivery vectors. Among the promising nanocarriers, magnetic nanoparticles (MNPs), such as Fe_3O_4 nanospheres, have more advantages, such as tumor tracing,[31,32] because of their magnetism and use in high-sensitivity real-time magnetic resonance imaging (MRI).[33,34]

The first two authors contributed equally to this work
[1]MOE Key Laboratory of Bioinformatics, School of Life Sciences, Tsinghua University, Beijing, China; [2]Key Laboratory of Advanced Materials of Ministry of Education of China, School of Materials Science & Engineering, Tsinghua University, Beijing, China; [3]Bioinformatics Division/Center for Synthetic & Systems Biology, Tsinghua National Laboratory for Information Science and Technology, Tsinghua University, Beijing, China; [4]MOE Key Laboratory of Bioinformatics, Department of Automation, Tsinghua University, Beijing, China. Correspondence: Qiong Wu, School of Life Sciences, Tsinghua University, Beijing 100084, China. E-mail: wuqiong@mail.tsinghua.edu.cn
Keywords: *in vivo* cancer therapy; magnetic nanoparticles; microRNA recognition system; tumor-specific
Received 24 August 2015; accepted 22 March 2016; advance online publication 3 May 2016. doi:10.1038/mtna.2016.28

Modified MNPs carriers have attracted increasing attention when combined with anticancer chemotherapeutics[35,36] or gene therapies.[37,38] For example, polyethyleneimine (PEI)-modified nanoparticles can condense with electronegative DNA molecules for DNA transfection[39,40] and thus facilitate gene delivery in cancer therapy.[41,42]

In this study, the ability to precisely pinpoint the miRNA patterns of cancer cells was investigated by increasing the number of cascades and types of miRNAs that were used to identify cancer cells. A cascade genetic system containing three plasmids, including a Tet activator, a lacI repressor gene driven by the TetOn promoter, and a reporter gene repressed by the lacI repressor with miRNA pairing sites was used to recognize the abnormal expression of miR-21, miR-9, and miR-145 in the human breast cancer cell line MCF-7 and to activate the expression of either a reporter gene (fluorescent protein) or the anticancer gene p53 (**Figure 1**). Moreover, this system was combined with PEI-modified MNPs and used to selectively kill cancer cells *in vivo*. This system was evaluated regarding its efficiency in selecting cells with miRNAs that were considered abnormal and for its efficacy in combination with the MNP carrier. For *in vitro* experiments based on cancer or normal cell lines and using fluorescence as a readout, the system showed up to an 3.2-fold greater fluorescence signal in the breast cancer cell line MCF-7 compared with the breast normal cell line HBL100. In an *in vivo* tumor experiment, however, the volume and weight of tumors in nude mice decreased to just 58 % of that in the control. This system shows potential in cancer therapy, and wide applications might be possible in the future when more complex recognition elements are developed.

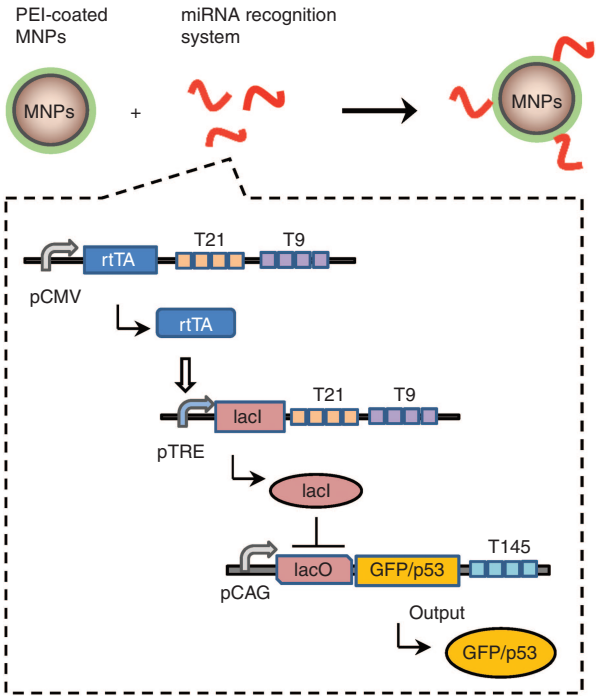

Figure 1 A schematic representation of the cascade system for accurate tumor targeting. PEI-coated MNPs were used to deliver plasmids that expressed the corresponding mRNA with miRNA pairing sites (T9, T21, and T145) that recognize specific endogenous miRNA (miR-9, miR-21, and miR-145, respectively) in tumor cells. miRNA, microRNAs; MNP, magnetic nanoparticles; PEI, polyethyleneimine; T9, miR-9 pairing sites; T21, miR-21 pairing sites; T145, miR-145 pairing sites.

Results

Design of a miRNA recognition system with cancer-cell-targeting ability

The miRNA recognition system consisted of plasmids containing several repeated DNA sequences pairing to corresponding miRNAs that were located in the 3′-untranslated regions of the respective genes of interest. When these plasmids were transcribed into mRNA in cells, these sites paired with relevant endogenous miRNAs and thus inhibited the expression of the genes of interest. A dual-luciferase assay demonstrated this function, as the ratio of the relative light units of firefly luciferase and Renilla clearly decreased when exogenous miRNA was added (see **Supplementary Figure S1**). In our study, a cascade miRNA recognition system structure, similar to that demonstrated in previous work, was used.[24] This system contained a Tet activator, a lacI repressor gene driven by the TetOn promoter and a reporter gene repressed by the lacI repressor so that when the designed miRNAs paired, the reporter's fluorescence protein and p53 were activated (**Figures 1** and **2**).

As previously reported, upregulated miR-21 facilitates cell growth in breast cancers[14,43,44] and many other diseases, including lung cancer and gastric cancer.[13,45,46] On the basis of these findings, tissue samples of lung, liver, muscle, and tumor were analyzed by total RNA extraction and miRNA quantitative real-time polymerase chain reaction (qRT-PCR). We confirmed that miR-21 was clearly overexpressed in tumors, at 5 to 16-fold higher than that in muscle, which had the lowest miR-21 levels (**Figure 3a**). The same experiment was performed in the human breast cancer cell line MCF-7 and the human epithelial cell line HBL100, in which the miR-21 expression level was 2.9-fold higher than that in MCF-7 (**Figure 3c**).

Generally, the presence of only one abnormal miRNA cannot lead to cancer, and typically several miRNAs that are abnormally up or downregulated in cancer.[16–18] Consequently, an additional miR-145 recognition site was added in the recognition system. qRT-PCR data confirmed the tumor suppressor function of miR-145 by a 5 to 10-fold decrease in tumor samples (**Figure 3b**) and a 0.25-fold decrease in the MCF-7 cell line compared with the levels in HBL100 (**Figure 3c**). Thus, in this study, miR-21 and miR-145 were chosen as the main markers.

The miRNA recognition system senses the artificially changed quantities of targeted miRNAs

Because miRNA functions by pairing with mRNA,[11] the simplest element with four repeats of the miR-21 pairing site downstream of the EGFP sequence (GFP-T21) was used to test the recognition ability (**Figure 4a**). After addition of exogenous miR-21, the fluorescence clearly decreased (**Figure 4b**), with an inhibition ratio of 91 % (**Figure 4c**), and the western blotting measurement also demonstrated this result (**Figure 4d**). The inhibition ratio varied depending

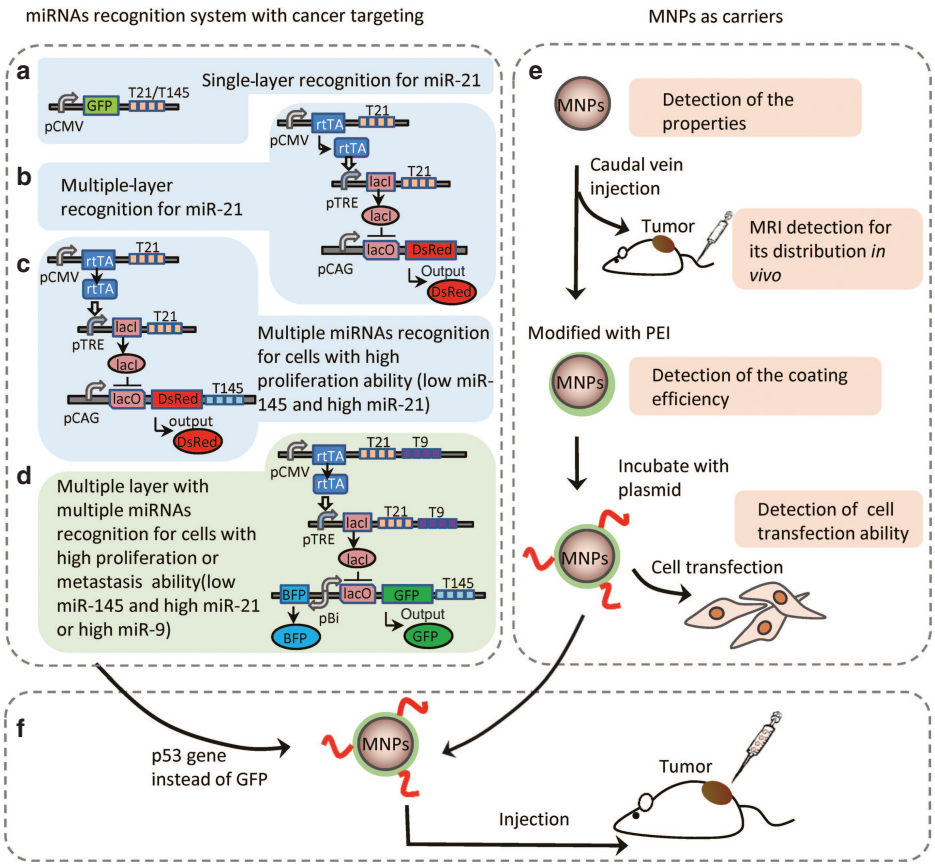

Figure 2 The experimental process. Tumor-specific miRNAs were chosen, and a recognition system was constructed to identify tumor cells. The structure of the miRNA recognition system was determined by experiments with a single cascade for single miRNA (**a**), multiple cascades for single miRNA (**b**), and multiple cascades for multiple miRNAs (**c**) in HEK293T cells by transfecting with exogenous miRNA mimics or inhibitors. Then, a cascade system that was used to recognize cells with high proliferation and metastasis ability was tested in the human breast cancer cell line MCF-7 and the human normal breast epithelial cell line HBL100 (**d**). The mechanical properties of MNPs were characterized, and PEI was surface coated to deliver the plasmid (**e**). The system that contained three cascades with the recognition of three miRNAs was finally delivered by PEI-coated MNPs for an *in vivo* test (**f**). miRNA, microRNAs; MNP, magnetic nanoparticles; PEI, polyethyleneimine.

on the type of miRNA and was relatively lower for miR-145, where it reached only 40 % (**Figure 4c**). Further experiments were performed to confirm that endogenous miRNAs also inhibited such a designed recognition sequence. The pEGFP-N1 plasmid with a miRNA pairing site downstream (GFP-T9, GFP-T21, and GFP-T145) exhibited decreased fluorescence compared with that of the control (see **Supplementary Figure S2**).

However, a system based on only one layer of miRNA recognition may lack stability and may be unreliable; thus, we addressed whether a multiple-cascade system could be used to more reliably distinguish cells with abnormal miRNAs. A cascade-inducible system was used in the following experiments, as shown in **Figure 4e**. We used only miR-21 at first and marked the layer that had the pairing site as "1" and that without the site as "0". In this way, the system was marked as (1, 1) or (0, 0). Regardless of whether exogenous miR-21 was added, the HEK293T cells generated almost the same fluorescence as with the (0, 0) system, *i.e.*, without miRNA recognition (**Figure 4f**). When recognition was added (*i.e.*, the (1, 1) system), the fluorescence of cells with exogenous miR-21 was 3.4 times stronger than that of the control (**Figure 4f**), and the difference was visible to the naked eye (**Figure 4g**). After addition of multi-miRNA recognition in parallel (*i.e.*, (1+) in **Supplementary Figure S3a**), the combination of different miRNAs showed a better inhibition effect (see **Supplementary Figure S3b**) and hence was used in the later design.

Given the complexity of cancer cells, miR-145 was included in the system as an additional control point, as shown in **Figure 4h**, yielding a configuration of the system as (1, 1, 1). A cell with high miR-21 and low miR-145 was considered to be a cancer cell in our study, and the results indicated that this system caused the mimicked cancer cells to express more fluorescent protein to levels 23.8 times higher than those in normal cells, thus widening the selectivity gap (**Figure 4i,j**).

The miRNA recognition system distinguishes cancer cells and normal cells in their natural state

Next, we sought to determine whether this system could be used to distinguish real cancer cells from normal cells. An additional cascade consisting of miR-9 recognition sites was added to the former two cascades because miR-9 promotes the invasion and metastasis of cancer cells *in vivo*.[47]

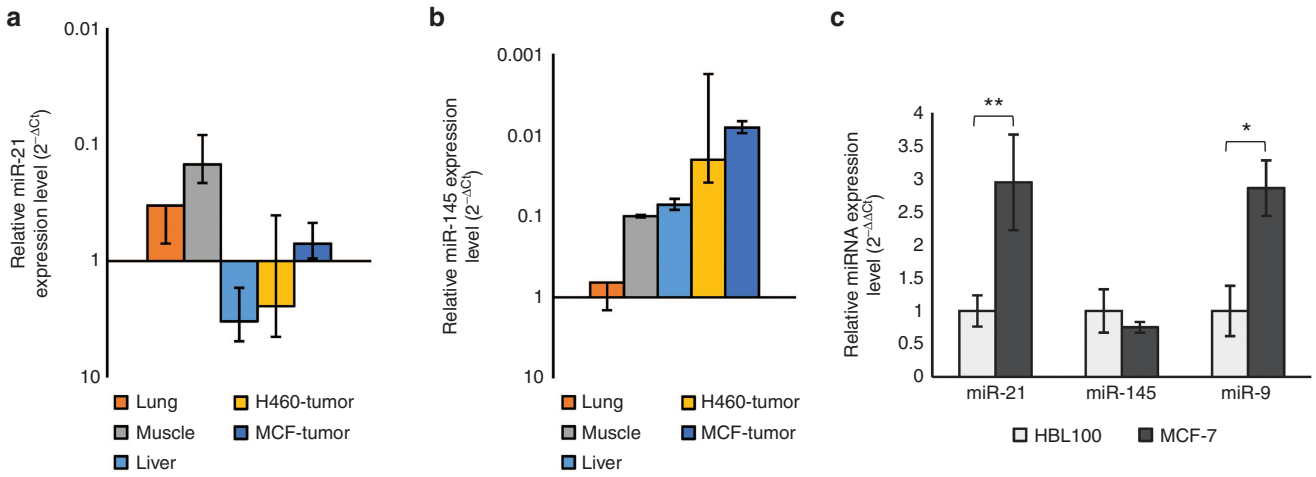

Figure 3 Measurement of miRNA quantities in cancer cells and normal cells. (**a**) Relative miR-21 expression level in normal tissue and human tumor cell xenograft samples from nude mice, as measured by qRT-PCR. The data are shown in logarithmic coordinates, and the *y*-axis is in reverse order (mean ± SD, $n = 4$). (**b**) The relative miR-145 expression level in normal tissue and human tumor cell xenograft samples from nude mice, as measured by qRT-PCR. The data are shown in logarithmic coordinates, and the *y*-axis is in reverse order (mean ± SD, $n = 4$). H460-tumor, xenograft samples made by injecting the human lung cancer H460 cell line; MCF-tumor, xenograft samples made by injecting the human breast cancer MCF-7 cell line. (**c**) qRT-PCR data of miR-21 and miR-145 in the human breast cancer MCF-7 cell line and the human normal breast epithelial HBL100 cell line. The results of MCF-7 are compared with data from HBL100 (mean ± SD, $n = 3$. $^{**}P < 0.01$, two-tailed *t*-test). miRNA, microRNAs; qRT-PCR, quantitative real-time polymerase chain reaction.

A transwell assay allowed the cells to grow on the upper membrane of the chamber and migrate to the lower channel (see **Supplementary Figure S4a**). Almost three times more cells migrated to the lower channel of the chamber membrane in cells transfected with exogenous miR-9 compared with control cells (see **Supplementary Figure S4b**). Thus, the system was updated as (1+, 1+, 1) (**Figure 5a**). The addition of the cascade system produced better recognition ability but still could not distinguish cancer cells from normal cells, because of the variable transfection efficiency (data not shown). Thus a blue fluorescent protein-encoding sequence that was not influenced by miRNA was added to normalize the results (**Figure 5a**); hence, the index *I* = green fluorescent protein/blue fluorescent protein was expected to be higher in cancer cells than in normal cells. This final system was tested in different cell lines, and this index was up to 7.5 in MCF-7 cells, much higher than in HBL100 and HEK293T cells, which had values of only 2.3 and 1, respectively (**Figure 5b,c**). These results thus demonstrated that the miRNA recognition system can indeed be used to accurately distinguish cancer cells from normal cells.

The p53 reporter gene in cancer cells and normal cells

Initially, the RNAe technique[48] was used to determine the most effective gene among several death-related genes according to their kill rate toward MCF-7, and the results indicated that p53 was the most effective one (**Figure 6a**). Consequently, the green fluorescent protein-encoding sequence was replaced with this effective death-related gene to form a killing system (**Figure 6b**). A system with miRNA recognition and the p53 reporter was tested with a CCK8 assay, as described in the methods, in HEK293T cells with exogenous miRNA expression (see **Supplementary Figure S5a,b**). Then, breast cancer cells MCF-7 and normal breast epithelial cells HBL100 were transfected with the system shown in **Figure 6b**. This system killed MCF-7 with an efficiency of 56 % (**Figure 6c**). Moreover, the killing system also more effectively inhibited the growth of MCF-7 cells with the overexpression of miR-9, thus indicating metastasizing cancer cells (see **Supplementary Figure S5c,d**).

MNPs accumulate in tumors via passive targeting

MNPs of 20–30 nm in diameter were prepared according to our previous work[49] and showed good morphological properties regarding their enhanced permeability and retention effect for tumor site targeting, as well as powerful magnetic properties for *in vivo* imaging. The morphology and structure of the MNPs were investigated by scanning electron microscopy and transmission electron microscopy. Representative scanning electron microscopy images (**Figure 7a**) showed that the MNP products were well dispersed and uniform, as confirmed by transmission electron microscopy images (**Figure 7b**).

The phase structure of the MNPs was identified by X-ray diffraction experiments (**Figure 7c**). The peaks obtained in the X-ray diffraction pattern matched those of Fe_3O_4 (JCPDS Card no. 39–1246). Additional magnetic properties of the MNPs were measured with a vibrating sample magnetometer at room temperature (**Figure 7d**). The magnetization curves displayed a relatively high saturation of magnetization (Ms) of ~85 emu/g.

To determine whether the MNPs could reach the tumor sites, a suspension was injected into the caudal veins of 7-week-old female BALB/c-nude mice with tumors that had been implanted 3 weeks prior. MRI images showed that most of the MNPs accumulated in the tumor over time (**Figure 7e**).

To deliver nucleic acids for *in vivo* cancer therapy, PEI was coated onto the surface of MNPs (**Figure 7f**). PEI-coated MNPs were very effective in carrying DNA when mixed with the pEGFP-N1 plasmid, as revealed by electrophoresis (see

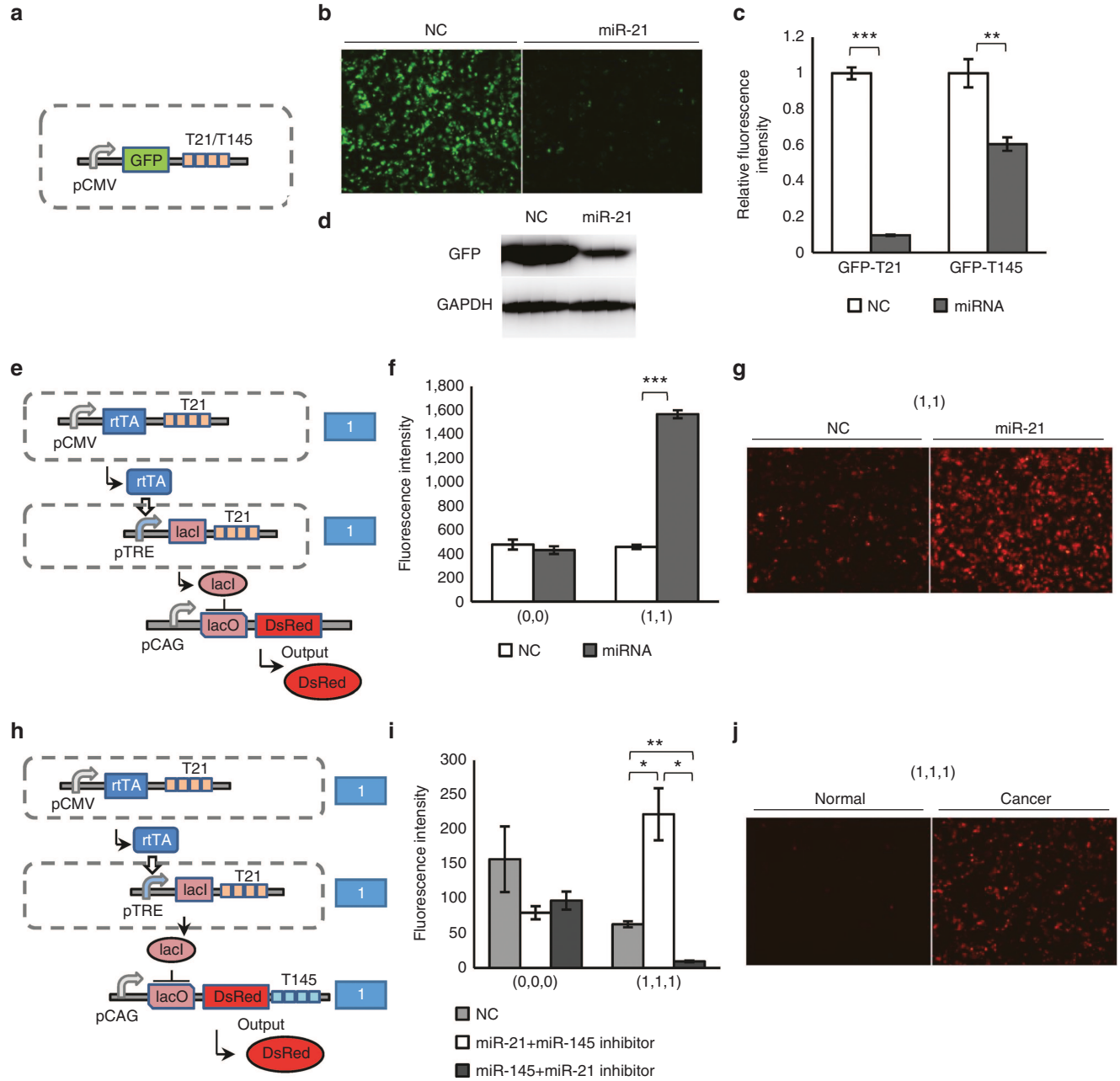

Figure 4 Functional test of the miRNA recognition system with single cascade with single miRNA recognition (a–d), multiple cascades with single-miRNA recognition (e–g) or multiple cascades with multiple-miRNA recognition (h–j). (**a**) Schematic of the single cascade with the single-miRNA recognition system. (**b**) Fluorescence image of HEK293T cells after transfection with the single-miRNA recognition system shown in **a** with exogenous miR-21 or negative control (NC). (**c**) The inhibition ratio of the single-miRNA recognition system for miR-21 or miR-145 as measured by flow cytometry. The result of respective plasmids with exogenous miRNAs was normalized to that with NC (mean ± SD, $n = 3$. $^{**}P < 0.01$, $^{***}P < 0.001$, two-tailed *t*-test). (**d**) The inhibition ratio of the single-miRNA recognition system for miR-21 with exogenous miR-21 or negative control (NC) as measured by western blotting. (**e**) Schematic of multiple layers with the single-miRNA recognition system. (**f**) Relative fluorescence level of HEK293T cells transfected with the system with (1, 1) or without (0, 0) miRNA recognition when exogenous miR-21 or negative control (NC) were added, as measured by flow cytometry (mean ± SD, $n = 3$. $^{**}P < 0.01$, two-tailed *t*-test). (**g**) Fluorescence image of HEK293T cells after transfection with the system with exogenous miR-21 or negative control (NC). (**h**) Schematic of multiple cascades with the multiple-miRNA recognition system. (**i**) Relative fluorescence intensity of HEK293T cells transfected with the system with (1, 1, 1) or without (0, 0, 0) miRNA recognition when adding exogenous miRNAs or negative control (NC), as measured by flow cytometry (mean ± SD, $n = 3$. $^{**}P < 0.01$, $^{***}P < 0.001$, two-tailed *t*-test). (**j**) Fluorescence image of HEK293T cells after transfection with the system with exogenous miRNA mimics or inhibitor. These three plasmids in each cascade were transfected with a mass ratio of 3:3:4 from the top to bottom of the cascade, and all of the plasmids and miRNA mimics or inhibitors were transfected using Lipofectamine 3000. miRNA, microRNAs.

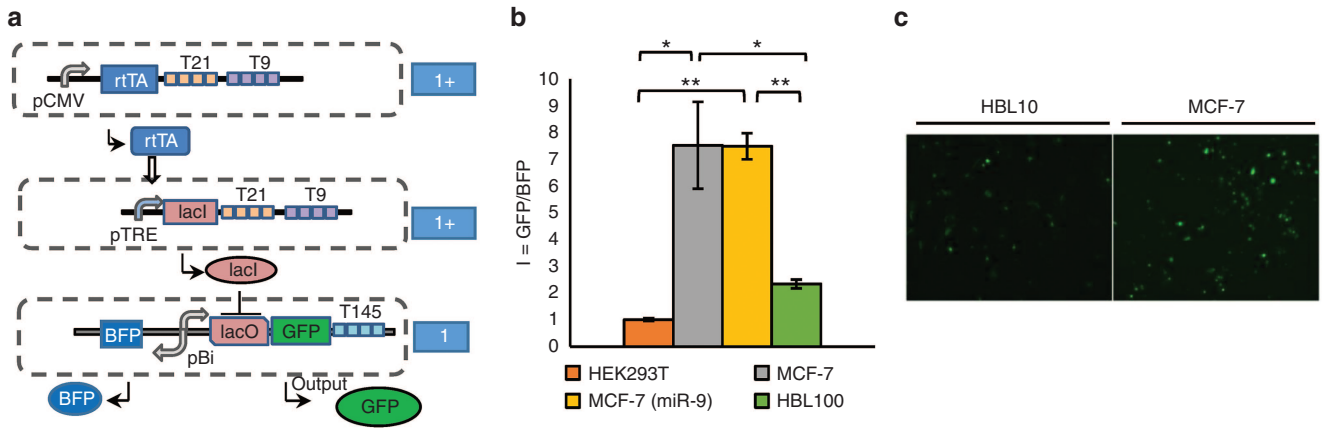

Figure 5 Functional test of the miRNA recognition system with miR-9 pairing sites (T9) in different cell lines. (**a**) Schematic of the miRNA recognition system with three types of miRNA recognition sites and three cascades. (**b**) Relative fluorescence fold (*I* = GFP/BFP) of the four cell lines (HEK293T, MCF-7, HBL100, and MCF-7 with lentivirus-based miR-9 overexpression) transfected with the system shown in **a**. The fluorescence intensity as measured by flow cytometry was normalized to the respective control, and the ratio of GFP minus BFP was calculated (mean ± SD, $n = 3$. $^{*}P < 0.05$, $^{**}P < 0.01$, two-tailed *t*-test). (c) Fluorescence image of GFP in MCF-7 and HBL100 cells transfected with the recognition system shown in **a.** BFP, blue fluorescent protein; GFP, green fluorescent protein; miRNA, microRNAs.

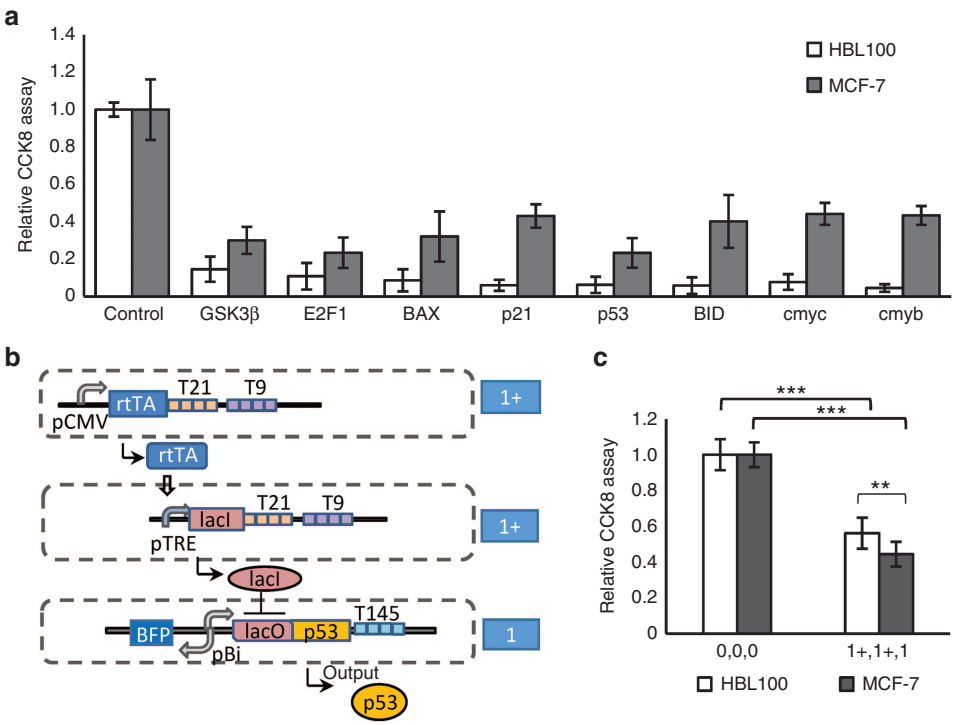

Figure 6 Experiments on the miRNA recognition system with a death-related protein *in vitro*. (**a**) Screening of a death-related protein by the RNAe method, as measured by a CCK8 assay (mean ± SD, $n = 7$). (**b**) The sketch map of the killing system, which contained three cascades with three miRNAs recognition and p53 tumor suppressor genes as the reporters. (**c**) The killing effect of the system with the p53 effector toward MCF-7 and HBL100 cells (mean ± SD, $n = 8$. $^{**}P < 0.01$, $^{***}P < 0.001$, two-tailed *t*-test). CCK8, cell proliferation and apoptosis analysis; miRNA, microRNAs.

Supplementary Figure S6a,b), and had relatively low aggregation (see **Supplementary Figure S6c,d**) and very low cytotoxicity (**Figure 7g**). Fluorescence microscopy demonstrated that the pEGFP-N1 plasmids could be transfected into HEK293T cells by the as-prepared MNPs with a relatively high efficiency compared with that of the plasmids alone (**Figure 7h**), indicating that the surface conjugation of plasmids onto MNPs is a feasible miRNA recognition system based on MNPs.

MNPs as carriers that accurately target and kill cancer cells *in vivo*.

By incubating the killing system shown in **Figure 6b** with MNPs, a tumor-targeted gene delivery system was constructed. When the product was injected around the tumor sites of 7-week-old female BALB/c-nude mice with xenograft tumors, as shown in **Figure 8a**, nanoparticles with an empty plasmid (pEGFP-C1 plasmid as a negative control) were

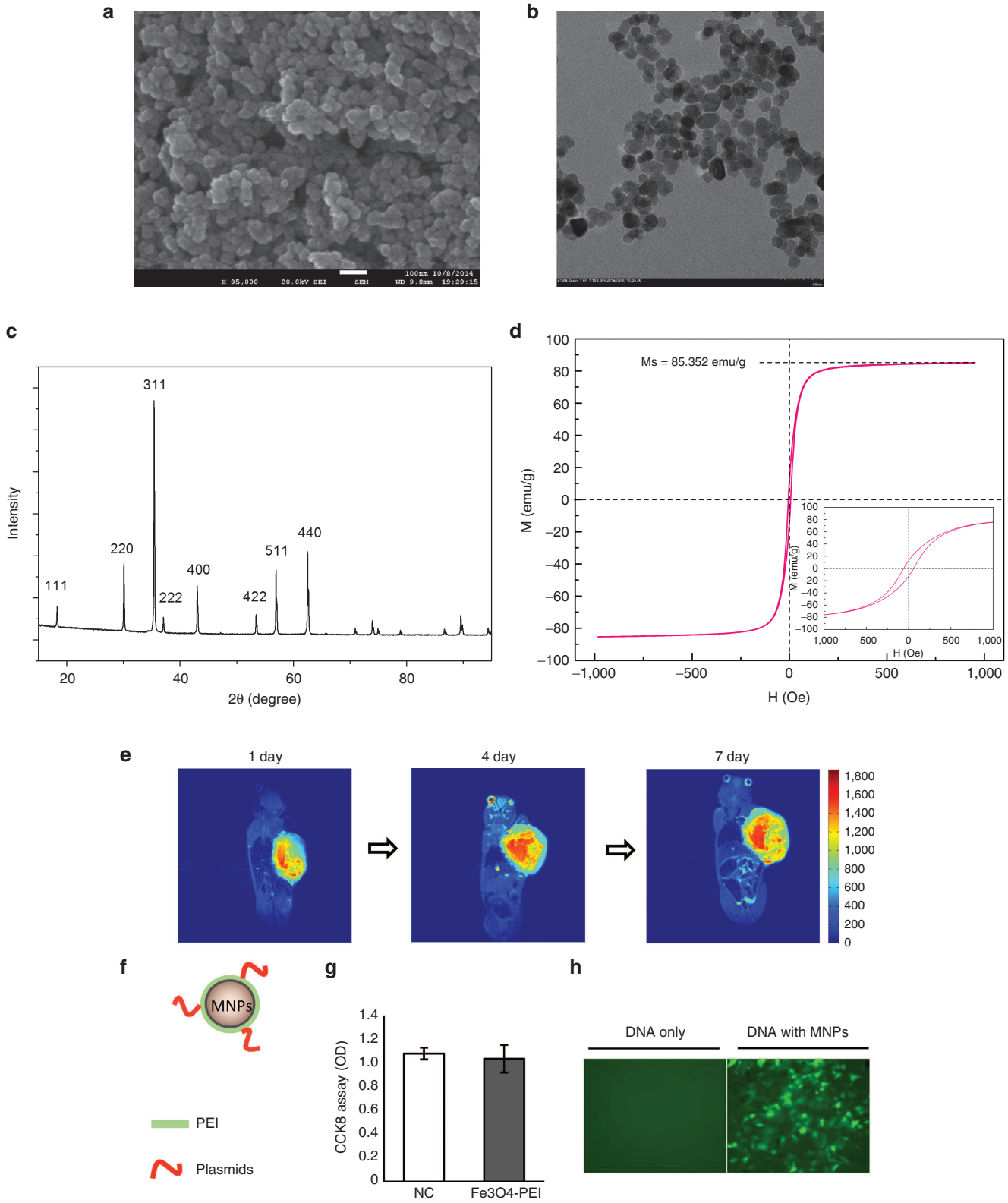

Figure 7 Assessment of MNPs. (**a**) Scanning electron microscopy (SEM) results. (**b**) Transmission electron microscopy (TEM) results. (**c**) X-ray diffraction (XRD) results. (**d**) Vibrating sample magnetometer (VSM) results. (**e**) Magnetic resonance imaging (MRI) results for the distribution of magnetic nanoparticles (MNPs) *in vivo*. Images were recorded at 1, 4, and 7 days after caudal vein injection. (**f**) Sketch map of the structure of polyethyleneimine (PEI)-modified MNPs after incubation with plasmids. (**g**) Cytotoxicity of PEI-modified Fe_3O_4 nanoparticles. (**h**) Fluorescence image of HEK293T cells transfected with DNA (pEGFP-N1) only or PEI-coated MNPs loaded with DNA.

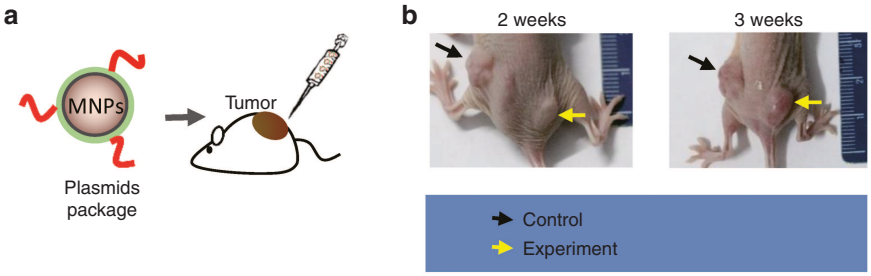

c

No.	1	2	3	4	5	Average
Control	0.2117	0.3195	0.4424	0.6882	0.7984	**0.492 ± 0.247**
Experiment	0.046	0.1968	0.2985	0.6345	0.3597	**0.307 ± 0.218**
Weight ratio	**0.217**	**0.616**	**0.675**	**0.922**	**0.451**	**0.576 ± 0.262***

Figure 8 Experiments on the killing system *in vivo*. (a) Schematic for applying the system *in vivo*. (b) An image of the tumor volume of an animal model injected with the pEGFP-N1 plasmid (left, black arrow) or the killing system (right, yellow arrow) shown in **Figure 6b** carried by PEI-coated MNPs. (c) Tumor weights of the animal models in the control (pEGFP-N1 plasmid carried by PEI-coated MNPs) or experimental (killing system shown in **Figure 6b** carried by PEI-coated MNPs) groups 4 weeks after injection. MNPs, magnetic nanoparticles; PEI, polyethyleneimine.

injected into the left tumor area, and nanoparticles with an equal amount of recognition system plasmids were injected into the right tumor area. The tumor was clearly smaller than that of the control (**Figure 8b**), and the tumor weight decreased almost 42 % after 4 weeks (**Figure 8c**).

Discussion

miRNAs are important components of cellular regulation networks.[11] In cancer cells, miRNAs also play an important role in the regulation of cell proliferation and migration processes.[16–19] Many miRNAs are considered to be oncogenic, including miR-21, which inhibits tumor suppressor gene tropomyosin 1 and programmed cell death 4, as well as many other genes, and thus affect tumor growth and apoptosis, respectively.[43,44,50] Some miRNAs can also act as tumor suppressor genes and are downregulated in most cancer cells. For example, miR-145 suppresses tumor growth by inhibiting insulin receptor substrate-1 and other genes, subsequently inducing cell death.[52,53] Although some miRNAs can be used as biomarkers for cancer diagnosis, different cancer cell lines also have their own miRNA expression patterns. In other words, the miRNA expression varies depending on an individual's exact cancer circumstances;[12,55] thus, for each cancer treatment, miRNA expression would need to be measured before construction of the recognition system, and genes with significant expression differences could then be selected as candidates. However, because miRNAs have complicated functional roles in various cellular processes, some onco-miRNAs may also be expressed in normal tissue. For example, miR-21 has a high expression level in the liver (**Figure 3a**) because miR-21 also plays a functional role in hepatocyte proliferation and liver regeneration.[56] Because of the lack of broad applicability and selectivity of single-miRNA systems, multi-miRNA recognition to identify cancer cells is necessary.

miRNA expression not only varies between cancer cells and normal cells but also changes when cancers transition into different states.[55] miRNAs also play a significant role in tumor state transformation, thus potentially allowing for precise personalized treatment. For example, miR-9 is a marker of tumor metastasis.[43,57,58] Using different miRNAs that mark different tumor states could also assist in the development of further specific treatments for different types of cancer.

The specificity of miRNA expression in tumors was supported by both a functional study and experimental data. With recent advances in biotechnology, both the detection time and cost required to determine miRNA expression levels (less than 1 day by qRT-PCR or by miRNA chip) decreased.[59,60] It may soon be possible to measure a cancer patients' miRNA expression levels in tumor and normal cells after surgery and to use this information to direct further personalized treatment to kill residual cancer cells via this recognition system method.

In our experiment, onco-miR miR-21 and tumor suppressor-miR miR-145 were used as model markers of cancer cells, which we defined as cells with high miR-21 and low miR-145 (**Figure 4h–j**). For experiments with cell lines in their natural state and for experiments *in vivo*, miR-9 was added to provide an alternative means to select the metastasizing cancer cells (**Figure 5**). Thus, we used HEK293T cells for the preliminary test because these cells have a weak tumorigenesis tendency and have been used in numerous research projects as somatic cell models. The measurement of miRNA expression in HEK293T cells indicated a low level of both miR-21 and miR-145. Thus, we considered the HEK293T cells with exogenous miR-21 mimics and the miR-145 inhibitor to be cancerous cell models and those with the exogenous miR-21 inhibitor and miR-145 mimics to be noncancerous, *i.e.*, normal, cell models.

Our work used a cascade recognition system consisting of three cascades and three types of miRNA recognition sites.

This system includes a miRNA-targeted rtTA expression plasmid, a miRNA-targeted Lac repressor (lacI) expression plasmid using the TetOn system and a miRNA/non-miRNA-targeted reporter gene expression plasmid controlled by lacI, as previously reported.[24,61] This system showed good performance in distinguishing HeLa and non-HeLa cells, as previously reported[24] and also distinguished between breast cancer cells and normal cells that were relatively similar in miRNA profile (**Figure 5c**). By replacing the sequence of miRNA pairing sites, the system can be made more specific and workable for particular cancer states. However, the structure of the miRNA recognition system still needs to be optimized by incorporating novel gene elements to improve accuracy.

Because different tumor suppressor genes have shown varying efficiencies in different tumor cell lines, the RNAe method[44] was used to screen and select promising genes for personalized treatments. The experimental data (**Figure 6a**) showed that among all of the selected genes, p53 was the best candidate to suppress MCF-7 cell growth. The p53 gene is the cellular gatekeeper for growth and division;[62] it has shown strong growth inhibition in some cases of cancer treatment,[63,64] and adenovirus-mediated p53 expression has been used as a treatment in clinical cancer therapy. However, because of a dominant negative mutation[65] or metabolic engineering pathway change, the p53 gene may have an inhibitory effect in some cases.[64] These results indicate that prescreening tumor suppressor genes before treatment can help to avoid low-efficiency tumor inhibition after treatment, which usually arises because of the diversity of cancer cells, even between different tumors of the same general type and morphology.

Personalized cancer treatments have become a major focus in cancer therapy. Because cancer cells display rapid and random mutations, different types of cancers and cancer cell types or even one cancer cell type in different states may have different gene expression and metabolic networks.[66,67] For traditional therapy methods, it is difficult to identify specific chemical or genetic medicines that can kill all cancers; thus, the investigation of novel designated strategies for personalized therapy has been proposed. The recognition of personalized cancers using biomarkers (such as the cancer specific metabolic pathway,[68] surface molecules,[69] or miRNAs)[24] to construct self-adaptation cancer treatment systems is one of the most promising concepts for future personalized treatment. In this work, details of miRNA selection based on cancer types and the selection of effector genes based on the RNAe method were provided and may make personalized practical applications considerably more feasible. However, in our experimental data (**Figure 6c**), there seemed to be no major difference between killing of MFC-7 and HBL100, possibly because the miR-21 expression level was not much higher (*e.g.*, 10–100 times) in these cells. In fact, when normal cells become cancerous, initial differences are minor. Thus, the killing system is designed to distinguish between cells that have highly similar miRNA expression levels. Although the killing efficiency was only slightly higher in MCF-7 than in HBL100 cells, the possible future clinical significance is that more kills targeting cancer cells would translate to a higher cure rate. In addition, the recognition system depends on plasmids that can be delivered in combination with biomedical material carriers to synergistically enhance the advantages. This system can also combine well with other biomedical materials via DNA delivery, which would allow its use to be broadened by choosing appropriate materials with different properties according to the tasks at hand. Finally, an integrated method was used for the preparation of PEI-modified MNPs for an *in vivo* cancer treatment test. This method was indeed confirmed to work well in tumor suppression, demonstrating its potential for future clinical use.

A suitable delivery method is also important for this recognition system's effect in *in vivo* tumor therapy. Nanoparticles smaller than 100 nm in diameter are suitable for cancer therapy because they can penetrate blood vessels only at tumor sites because of the enhanced permeability and retention effect[33] and thus can target the tumor site passively as carriers for cancer therapy. MNPs of ~20–30 nm in diameter fit well (**Figure 7a**,b) and, in our experiment, showed significant accumulation at the tumor site (**Figure 7e**). Conveniently, MNPs, in addition to carrying medicines, can also be detected by MRI imaging,[31,32] which can aid in cancer diagnosis. MRI images can also be used to determine the residual quantity, which may also help in dosage control of the injected nanoparticles.

When coated with PEI, MNPs showed significant condensation efficiency and transfection effects on target cells. Various polymers with electropositivity have been selected in a previous study.[70] Among these polymers, PEI shows better affinity to cell membranes than does PEG or several other materials, when coated on the surface of nanoparticles.[71] Furthermore, the copolymerization of various monomers may improve the material properties by combining advantages of different monomers. For example, Kievit *et al.*[72] have reported that copolymers of PEI, PEG, and chitosan show better properties because chitosan prevents nanoparticles from aggregating,[73] PEG shields the nanoparticles from the immune system,[74] and PEI can condense DNA and deliver it into cells.[71] Future improvement of the surface modification process and of the design of MNPs with multifunctional properties may further improve this therapeutic effect.

In conclusion, miRNAs differ in various tissues or cell types and can be used for specific cancer cell discrimination. An artificially designed miRNA recognition system was constructed to distinguish cells with exogenous miRNAs or different cell types in their natural state, on the basis of the quantities of different miRNAs. This system, with death-related gene p53 as an output, can more selectively suppress the growth of cancer cells for cancer treatment. MNPs coated with PEI showed good DNA carrying ability, biocompatibility, *in vivo* imaging, and plasmid delivery properties. Moreover, when delivered by PEI-coated MNPs, this system can kill cancer cells directly and specifically both in *in vitro* and *in vivo*. These results demonstrate that the miRNA recognition system combined with nanotechnology shows great potential for the future development of personalized cancer treatments.

Materials and methods

Cell culture. MCF-7, HBL100, and HEK293T cells were obtained from the Cell Resource Center, Peking Union Medical College and were cultured in Dulbecco's modified Eagle's medium (Corning, Manassas, Virginia) containing 10 % fetal bovine serum (Gibco, Grand Island, New York), 0.1 mg/ml

streptomycin (Inalco Pharmaceuticals, San Luis Obispo, California) and 0.1 mg/ml penicillin (Inalco Pharmaceuticals, San Luis Obispo, California). All of the cells were cultured under humidified conditions with 5 % CO_2 and 95 % air at 37 °C.

Synthesis of PEI-modified MNPs. Magnetic Fe_3O_4 nanospheres were synthesized according to Yan's protocol.[49] Briefly, 2 mmol ferric chloride hexahydrate ($FeCl_3 \cdot 6H_2O$, Tianjin Guangfu Technology Development, Tianjing, China) and 2 mmol of dodecylamine (Sinopharm Chemical Reagent, Shanghai, China) were added to 20 ml of ethylene glycol (Sinopharm Chemical Reagent, Shanghai, China)/diethylene glycol (Sinopharm Chemical Reagent, Shanghai, China) at a 3/1 (v/v) ratio and mixed under continuous stirring until completely dissolved. Separately, 4 mmol of NaOH was dissolved in 10 ml of the ethylene glycol/diethylene glycol mixed solvent in another flask. The solution of NaOH was added to the solution of iron chloride with stirring, causing an immediate color change from colorless to yellow. The resulting mixture was sealed into a 40-ml Teflon-lined autoclave, and this was followed by solvothermal treatment at 220 °C for 12 hours in an electric oven. The product was harvested by magnetic separation, washed with distilled water and absolute ethanol several times, and dried in a vacuum oven at 60 °C overnight. PEI powder (linear PEI, Mr = 5,000, Aladdin, Shanghai, China) and Fe_3O_4 nanospheres were dissolved in ethanol and dispersed for 30 minutes and 1 hour, respectively; by ultrasonication (JY92-II, Scientz Biotech, Ningbo, China). Then, these two solutions were mixed with high-power ultrasonic dispersion for 1 hour, accompanied by mechanical agitation. The product was washed three times with ethanol and dried in oven for 24 hours at 80 °C.[51,54]

Characterization of MNPs. Powder X-ray diffraction patterns were measured on an X-ray diffractometer (Bruker D8 Discover, Karlsruhe, Germany) using a Cu-Kα (l = 1.540562 Å, 40 kV, 40 mA) X-ray source. Scanning electron microscopy (JEOL JSM-7001F, Akishima City, Japan) and transmission electron microscopy (Hitachi HT7700, Tokyo, Japan) were used to characterize the morphology of the nanospheres. The magnetic properties of the product were investigated using a vibrating sample magnetometer (LakeShore 7307, Lake Elsinore, California) with an applied field between –10,000 and 10,000 Oe at room temperature.

Plasmid construction. Plasmids were as reported in our previous paper[48,75] or were obtained from Prof. Xie.[24] The antisense sequences of miR-145/miR-9 (T145/T9) were ordered as synthetic DNAs (Qinglan Biotech, Suzhou, China), which could pair with exogenous miR-145/miR-9 in cells after they were transcribed into RNAs. Their sequences are given in **Supplementary Table S1**. Related plasmids were constructed by general molecular biological techniques and are listed in **Supplementary Table S1**. For plasmid construction, restriction endonucleases (Thermo Scientific, Waltham, Massachusetts), T4 polynucleotide kinase (PNK, Thermo Scientific, Waltham, Massachusetts), T4 DNA ligase (Thermo Scientific, Waltham, Massachusetts), alkaline phosphatase (FastAP, Thermo Scientific, Waltham, Massachusetts), Taq polymerase (GenStar, Keruisixun Biotech, Beijing, China) and Q5 polymerase (New England BioLabs, Ipswich, UK) were used. All of the primers that were used for cloning are listed in **Supplementary Table S2**.

Cell transfection. For MCF-7 and HEK293T cell lines, cells were digested with 0.05 % trypsin (Gibco, New York, Grand Island) at 37 °C for 2 minutes and the reaction was terminated with cell culture medium as previously described. After centrifugation at room temperature at 1,000 rpm for 5 minutes and the resuspension of the cell precipitate, cells were passaged on 24-well plates (Corning, Manassas, Virginia). When the cell confluence reached 40–50 % (~1×10^5 cells), the cells were transfected with 0.5 μg of plasmid DNA with Lipofectamine 3000 reagent (Invitrogen, Carlsbad, California) per well according to the manufacturer's instructions. For the HBL100 cell line, nearly 2×10^6 cells were used and electroporation-based transfection was performed using a Nucleofector Kit (Lonza, Basel, Switzerland) and Nucleofector Devices (Lonza, Basel, Switzerland) following the manual. The culture medium was exchanged for medium containing 500 ng/ml doxycycline (Dox, Sigma Aldrich, St. Louis, Missouri) 12 hours after transfection. Moreover, miRNA mimics and inhibitors (GenePharma, Suzhou, China) were transfected with Lipofectamine 3000 reagent (Invitrogen, Carlsbad, California) according to the manufacturer's instructions.

Flow cytometry analysis. Cells were digested with 0.05 % trypsin (Gibco, Grand Island, New York) after induction for 48 hours and resuspended in phosphate buffer (PBS, HX-bio, Beijing, China) for flow cytometry analysis (BD LSRFortessa, San Jose, California) using the 405 nm (for blue fluorescent protein), 488 nm (for green fluorescent protein), and 561 nm (for DsRed) laser.

Preparation of PEI-modified MNPs carrier–plasmid complex and transfection. Plasmid DNA was mixed with PEI-modified MNPs at mass ratio of 1:3 in water solution and incubated for at least 4 hours at 4 °C. Cells were cultured and seeded in 24-well plate as described above. Subsequently, the medium was changed with Opti-MEM Reduced Serum Medium (Gibco, Grand Island, New York) and about 10 μg PEI-modified MNPs loaded with plasmid DNA were added to each well. After 5 hours, the medium was changed back to normal culture medium and the cells were incubated further for 48 hours. Pictures were taken using fluorescence inversion microscope (Nikon Eclipse T*i*, Tokyo, Japan).

Xenograft establishment. Animal experiments were executed according to the protocol approved by the Institutional Animal Care and Use guidelines from the IACUC of Tsinghua University, Beijing, China. Four-week-old female BALB/c-nude mice were implanted with 1 mm^3 tumor cubes from donor mice which were injected by 10^6 MCF-7 cells subcutaneously and raised for 4 weeks until tumor growth with an evident diameter of ~2 cm.

MRI detection. MCF-7 cells were digested with 0.05 % trypsin for 1–2 minutes and resuspended in PBS at a concentration of 1×10^7 cells /ml. Subsequently, 4-week-old female BALB/c nude mice were chosen and 0.1 ml of suspension was injected under the axillary skin. After 21 days (when the

tumor under axilla could be visualized significantly), the mice were anesthetized by a 1 % pentobarbital solution (1 ml/100 g weight) and injected with the PEI-modified MNPs (200 µl, 4.5 mmol/l) into the caudal vein. MRI images were acquired at 1, 4, and 7 days after injection. The T_2-map images were obtained from a clinical 3-T MRI scanner (Philips, Amsterdam, Netherlands), using the following settings: TR = 1,200 ms, TE = 30.2 ms, slice thickness = 2.5 mm.

Quantitative real-time polymerase chain reaction. Total RNA was isolated from cell lines and tissue samples by a miRcute mRNA Isolation Kit (Tiangen Biotech, Beijing, China). Subsequently, cDNA was synthesized using a miRcute miRNA First-Strand cDNA Synthesis kit (Tiangen Biotech, Beijing, China). qRT-PCR was performed using miRcute miRNA qPCR Detection kit (SYBR Green) (Tiangen Biotech, Beijing, China). U6 was used as the interior control for miRNA detection. The primers used for qRT-PCR were purchased from Tiangen Biotech Company (Beijing, China).

Cell proliferation and apoptosis analysis (CCK8 assay). Cells were seeded in 96-well plate and transfection was performed when cell confluence reaching 60–70 %. After cultured for 48 hours, cell culture medium was changed with fresh culture medium premixed with cell counting kit-8 reagent (CCK8, Beyotime, Shanghai, China) at ratio of 1/10 (v/v). Then the cells were incubated at 37 °C for about 1 hour and analyzed for absorbance by Varioskan Flash (Thermo Scientific, Waltham, Massachusetts) at wavelengths of 450 and 650 nm.

Statistical analysis. The paired two-tailed Student's *t*-test was used for statistical analysis. Results were represented as mean ($n \geq 3$) ± standard deviation. Values were considered significant at $P < 0.05$, $P < 0.01$ or $P < 0.001$ which were indicated with one, two or three stars, respectively.

Supplementary material

Figure S1. The dual-luciferase assay on miRNAs.
Figure S2. Function test on miRNA recognition system.
Figure S3. Function test on multi-miRNA (1+) recognition system.
Figure S4. Migration enhancement by miR-9 overexpression in Transwell experiment.
Figure S5. Killing effect of miRNAs recognition system on cells with abnormal miRNA quantities *in vitro*.
Figure S6. Experiments on the incubation of MNPs and plasmids.
Figure S7. Flow cytometry data of the experiments *in vivo*.
Table S1. Plasmids used in this work.
Table S2. Primers used in this work.

Acknowledgments The authors thank Ivan Hajnal (Tsinghua University, China) for help on literal revision. Y.Y. (Yu) and Y.Y. (Yao) developed and invented the method. Y.Y. (Yu), Y.Y. (Yao), R.W., Z.Z., and X.A. performed the *in vitro* experiments. H.Y., X.S., and L.Z. performed the preparation and physical properties measurement of Fe_3O_4 nanospheres. Y.Y. (Yao) and L.Z. performed the animal experiments. H.Z. and J.L. performed the screening experiments. Y.Y. (Yu) and Y.Y. (Yao) wrote the manuscript. Z. X. and Q.W. guided frame of the work and helped to analyze and check the data in this manuscript. This research was supported by Natural Sciences Foundation of China (Grant Nos. 31170940 and 31470933), 973 Basic Research Fund (Grant No. 2012CB725200), National High Technology Research and Development (863 Program) (Grant Nos. 2012AA020503, 2013AA020301, and 2012AA02A702), National Fund for Talent Training in Basic Science No. J1310020), Tsinghua University Initiative Scientific Research Program (No. 20131089199).

1. Siegel, R, Naishadham, D and Jemal, A (2012). Cancer statistics, 2012. *CA Cancer J Clin* **62**: 10–29.
2. Racioppi, M, D'Agostino, D, Totaro, A, Pinto, F, Sacco, E, D'Addessi, A *et al.* (2012). Value of current chemotherapy and surgery in advanced and metastatic bladder cancer. *Urol Int* **88**: 249–258.
3. Marta, GN, Hanna, SA, Gadia, R, Correa, SF, Silva, JL and Carvalho, Hde A (2012). The role of radiotherapy in urinary bladder cancer: current status. *Int Braz J Urol* **38**: 144–53; discussion 153.
4. Zhang, L, Fan, Y and Wu, Y (2014). Inositol based non-viral vectors for transgene expression in human cervical carcinoma and hepatoma cell lines. *Biomaterials* **35**: 2039–2050.
5. Park, H, Tsutsumi, H and Mihara, H (2013). Cell penetration and cell-selective drug delivery using α-helix peptides conjugated with gold nanoparticles. *Biomaterials* **34**: 4872–4879.
6. Wirth T and Ylä-Herttuala S. Gene therapy used in cancer treatment. *Biomedicines* 2014, **2**: 149–162.
7. Unger, FT, Witte, I and David, KA (2015). Prediction of individual response to anticancer therapy: historical and future perspectives. *Cell Mol Life Sci* **72**: 729–757.
8. Iorio, MV, Ferracin, M, Liu, CG, Veronese, A, Spizzo, R, Sabbioni, S *et al.* (2005). MicroRNA gene expression deregulation in human breast cancer. *Cancer Res* **65**: 7065–7070.
9. Yanaihara, N, Caplen, N, Bowman, E, Seike, M, Kumamoto, K, Yi, M *et al.* (2006). Unique microRNA molecular profiles in lung cancer diagnosis and prognosis. *Cancer Cell* **9**: 189–198.
10. Schetter, AJ, Leung, SY, Sohn, JJ, Zanetti, KA, Bowman, ED, Yanaihara, N *et al.* (2008). MicroRNA expression profiles associated with prognosis and therapeutic outcome in colon adenocarcinoma. *JAMA* **299**: 425–436.
11. He, L and Hannon, GJ (2004). MicroRNAs: small RNAs with a big role in gene regulation. *Nat Rev Genet* **5**: 522–531.
12. Lu, J, Getz, G, Miska, EA, Alvarez-Saavedra, E, Lamb, J, Peck, D *et al.* (2005). MicroRNA expression profiles classify human cancers. *Nature* **435**: 834–838.
13. Zhang, Z, Li, Z, Gao, C, Chen, P, Chen, J, Liu, W *et al.* (2008). miR-21 plays a pivotal role in gastric cancer pathogenesis and progression. *Lab Invest* **88**: 1358–1366.
14. Si, ML, Zhu, S, Wu, H, Lu, Z, Wu, F and Mo, YY (2007). miR-21-mediated tumor growth. *Oncogene* **26**: 2799–2803.
15. Medina, PP, Nolde, M and Slack, FJ (2010). OncomiR addiction in an *in vivo* model of microRNA-21-induced pre-B-cell lymphoma. *Nature* **467**: 86–90.
16. Esquela-Kerscher, A and Slack, FJ (2006). Oncomirs—microRNAs with a role in cancer. *Nat Rev Cancer* **6**: 259–269.
17. Calin, GA and Croce, CM (2006). MicroRNA signatures in human cancers. *Nat Rev Cancer* **6**: 857–866.
18. Zhang, B, Pan, X, Cobb, GP and Anderson, TA (2007). MicroRNAs as oncogenes and tumor suppressors. *Dev Biol* **302**: 1–12.
19. Ferracin, M, Veronese, A and Negrini, M (2010). Micromarkers: miRNAs in cancer diagnosis and prognosis. *Expert Rev Mol Diagn* **10**: 297–308.
20. Mansfield, JH, Harfe, BD, Nissen, R, Obenauer, J, Srineel, J, Chaudhuri, A *et al.* (2004). MicroRNA-responsive 'sensor' transgenes uncover Hox-like and other developmentally regulated patterns of vertebrate microRNA expression. *Nat Genet* **36**: 1079–1083.
21. Brown, BD, Gentner, B, Cantore, A, Colleoni, S, Amendola, M, Zingale, A *et al.* (2007). Endogenous microRNA can be broadly exploited to regulate transgene expression according to tissue, lineage and differentiation state. *Nat Biotechnol* **25**: 1457–1467.
22. Wu, C, Lin, J, Hong, M, Choudhury, Y, Balani, P, Leung, D *et al.* (2009). Combinatorial control of suicide gene expression by tissue-specific promoter and microRNA regulation for cancer therapy. *Mol Ther* **17**: 2058–2066.
23. Lee, CY, Rennie, PS and Jia, WW (2009). MicroRNA regulation of oncolytic herpes simplex virus-1 for selective killing of prostate cancer cells. *Clin Cancer Res* **15**: 5126–5135.
24. Xie, Z, Wroblewska, L, Prochazka, L, Weiss, R and Benenson, Y (2011). Multi-input RNAi-based logic circuit for identification of specific cancer cells. *Science* **333**: 1307–1311.
25. Kesharwani, P, Gajbhiye, V and Jain, NK (2012). A review of nanocarriers for the delivery of small interfering RNA. *Biomaterials* **33**: 7138–7150.
26. Oh, IH, Min, HS, Li, L, Tran, TH, Lee, YK, Kwon, IC *et al.* (2013). Cancer cell-specific photoactivity of pheophorbide a-glycol chitosan nanoparticles for photodynamic therapy in tumor-bearing mice. *Biomaterials* **34**: 6454–6463.

27. Kim, HA, Nam, K and Kim, SW (2014). Tumor targeting RGD conjugated bio-reducible polymer for VEGF siRNA expressing plasmid delivery. *Biomaterials* **35**: 7543–7552.
28. Yoshizaki, Y, Yuba, E, Sakaguchi, N, Koiwai, K, Harada, A and Kono, K (2014). Potentiation of pH-sensitive polymer-modified liposomes with cationic lipid inclusion as antigen delivery carriers for cancer immunotherapy. *Biomaterials* **35**: 8186–8196.
29. Matsumura, Y and Maeda, H (1986). A new concept for macromolecular therapeutics in cancer chemotherapy: mechanism of tumoritropic accumulation of proteins and the antitumor agent smancs. *Cancer Res* **46**: 6387–6392.
30. Alexis, F, Pridgen, E, Molnar, LK and Farokhzad, OC (2008). Factors affecting the clearance and biodistribution of polymeric nanoparticles. *Mol Pharm* **5**: 505–515.
31. Lin, G, Zhu, W, Yang, L, Wu, J, Lin, B, Xu, Y *et al.* (2014). Delivery of siRNA by MRI-visible nanovehicles to overcome drug resistance in MCF-7/ADR human breast cancer cells. *Biomaterials* **35**: 9495–9507.
32. Huang, KW, Chieh, JJ, Horng, HE, Hong, CY and Yang, HC (2012). Characteristics of magnetic labeling on liver tumors with anti-alpha-fetoprotein-mediated Fe3O4 magnetic nanoparticles. *Int J Nanomedicine* **7**: 2987–2996.
33. Huang, J, Bu, L, Xie, J, Chen, K, Cheng, Z, Li, X *et al.* (2010). Effects of nanoparticle size on cellular uptake and liver MRI with polyvinylpyrrolidone-coated iron oxide nanoparticles. *ACS Nano* **4**: 7151–7160.
34. Colombo, M, Carregal-Romero, S, Casula, MF, Gutiérrez, L, Morales, MP, Böhm, IB *et al.* (2012). Biological applications of magnetic nanoparticles. *Chem Soc Rev* **41**: 4306–4334.
35. Ren, Y, Zhang, H, Chen, B, Cheng, J, Cai, X, Liu, R *et al.* (2012). Multifunctional magnetic Fe3O4 nanoparticles combined with chemotherapy and hyperthermia to overcome multidrug resistance. *Int J Nanomedicine* **7**: 2261–2269.
36. Jain, TK, Morales, MA, Sahoo, SK, Leslie-Pelecky, DL and Labhasetwar, V (2005). Iron oxide nanoparticles for sustained delivery of anticancer agents. *Mol Pharm* **2**: 194–205.
37. Yiu, HH, Pickard, MR, Olariu, CI, Williams, SR, Chari, DM and Rosseinsky, MJ (2012). Fe3O4-PEI-RITC magnetic nanoparticles with imaging and gene transfer capability: development of a tool for neural cell transplantation therapies. *Pharm Res* **29**: 1328–1343.
38. McBain, SC, Yiu, HH and Dobson, J (2008). Magnetic nanoparticles for gene and drug delivery. *Int J Nanomedicine* **3**: 169–180.
39. Yiu HHP, McBain SC, El Haj AJ, Dobson J. A triple-layer design for polyethyleneimine-coated, nanostructured magnetic particles and their use in DNA binding and transfection. *Nanotechnology* 2007; **18**: 435601.
40. Kasturi, SP, Sachaphibulkij, K and Roy, K (2005). Covalent conjugation of polyethyleneimine on biodegradable microparticles for delivery of plasmid DNA vaccines. *Biomaterials* **26**: 6375–6385.
41. Yamano, S, Dai, J, Hanatani, S, Haku, K, Yamanaka, T, Ishioka, M *et al.* (2014). Long-term efficient gene delivery using polyethylenimine with modified Tat peptide. *Biomaterials* **35**: 1705–1715.
42. Liu, C, Liu, F, Feng, L, Li, M, Zhang, J and Zhang, N (2013). The targeted co-delivery of DNA and doxorubicin to tumor cells via multifunctional PEI-PEG based nanoparticles. *Biomaterials* **34**: 2547–2564.
43. Zhu, S, Si, ML, Wu, H and Mo, YY (2007). MicroRNA-21 targets the tumor suppressor gene tropomyosin 1 (TPM1). *J Biol Chem* **282**: 14328–14336.
44. Frankel, LB, Christoffersen, NR, Jacobsen, A, Lindow, M, Krogh, A and Lund, AH (2008). Programmed cell death 4 (PDCD4) is an important functional target of the microRNA miR-21 in breast cancer cells. *J Biol Chem* **283**: 1026–1033.
45. Seike, M, Goto, A, Okano, T, Bowman, ED, Schetter, AJ, Horikawa, I *et al.* (2009). MiR-21 is an EGFR-regulated anti-apoptotic factor in lung cancer in never-smokers. *Proc Natl Acad Sci USA* **106**: 12085–12090.
46. Slaby, O, Svoboda, M, Fabian, P, Smerdova, T, Knoflickova, D, Bednarikova, M *et al.* (2007). Altered expression of miR-21, miR-31, miR-143 and miR-145 is related to clinicopathologic features of colorectal cancer. *Oncology* **72**: 397–402.
47. Ma, L, Young, J, Prabhala, H, Pan, E, Mestdagh, P, Muth, D *et al.* (2010). miR-9, a MYC/MYCN-activated microRNA, regulates E-cadherin and cancer metastasis. *Nat Cell Biol* **12**: 247–256.
48. Yao, Y, Jin, S, Long, H, Yu, Y, Zhang, Z, Cheng, G, *et al.* (2015). RNAe: an effective method for targeted protein translation enhancement by artificial non-coding RNA with SINEB2 repeat. *Nucleic Acids Res* (in press).
49. Yan, H, Chen, Y, Sun, XD, Zhao, LY, Zhang, CX, Bian, L, *et al.* One-pot synthesis of size and structure-controllable Fe3O4 spheres with a high saturation magnetization as contrast agents for T2 magnetic resonance imaging. *Small* (submitted).
50. Meng, F, Henson, R, Wehbe-Janek, H, Ghoshal, K, Jacob, ST and Patel, T (2007). MicroRNA-21 regulates expression of the PTEN tumor suppressor gene in human hepatocellular cancer. *Gastroenterology* **133**: 647–658.
51. Benjamin T, Lucie Z, Scott M, Kim F, Christophe B, Hans JG. Electrostatic self-assembly of PEG copolymers onto porous silica nanoparticles. *Langmuir* 2008; **24**: 8143–8150.
52. Shi, B, Sepp-Lorenzino, L, Prisco, M, Linsley, P, deAngelis, T and Baserga, R (2007). Micro RNA 145 targets the insulin receptor substrate-1 and inhibits the growth of colon cancer cells. *J Biol Chem* **282**: 32582–32590.
53. Ostenfeld, MS, Bramsen, JB, Lamy, P, Villadsen, SB, Fristrup, N, Sørensen, KD *et al.* (2010). miR-145 induces caspase-dependent and -independent cell death in urothelial cancer cell lines with targeting of an expression signature present in Ta bladder tumors. *Oncogene* **29**: 1073–1084.
54. Sangyong J, Jiehyun S, Ali K, Thanh-Nga TT, Paul EL, Robert L. Construction of nonbiofouling surfaces by polymeric self-assembled monolayers. *Langmuir* **19**: 9989–9993.
55. Shingara, J, Keiger, K, Shelton, J, Laosinchai-Wolf, W, Powers, P, Conrad, R *et al.* (2005). An optimized isolation and labeling platform for accurate microRNA expression profiling. *RNA* **11**: 1461–1470.
56. Bai, YN, Yu, ZY, Luo, LX, Yi, J, Xia, QJ, Zeng, Y (2014). MicroRNA-21 accelerates hepatocyte proliferation in vitro via PI3K/Akt signaling by targeting PTEN. *Biochem Bioph Res Co* **443**: 802–807.
57. Khew-Goodall, Y and Goodall, GJ (2010). Myc-modulated miR-9 makes more metastases. *Nat Cell Biol* **12**: 209–211.
58. Zhu, L, Chen, H, Zhou, D, Li, D, Bai, R, Zheng, S *et al.* (2012). MicroRNA-9 up-regulation is involved in colorectal cancer metastasis via promoting cell motility. *Med Oncol* **29**: 1037–1043.
59. Li, J, Yao, B, Huang, H, Wang, Z, Sun, C, Fan, Y *et al.* (2009). Real-time polymerase chain reaction microRNA detection based on enzymatic stem-loop probes ligation. *Anal Chem* **81**: 5446–5451.
60. Yang, H, Hui, A, Pampalakis, G, Soleymani, L, Liu, FF, Sargent, EH *et al.* (2009). Direct, electronic microRNA detection for the rapid determination of differential expression profiles. *Angew Chem Int Ed Engl* **48**: 8461–8464.
61. Rinaudo, K, Bleris, L, Maddamsetti, R, Subramanian, S, Weiss, R and Benenson, Y (2007). A universal RNAi-based logic evaluator that operates in mammalian cells. *Nat Biotechnol* **25**: 795–801.
62. Levine, AJ (1997). p53, the cellular gatekeeper for growth and division. *Cell* **88**: 323–331.
63. Antonia, SJ, Mirza, N, Fricke, I, Chiappori, A, Thompson, P, Williams, N *et al.* (2006). Combination of p53 cancer vaccine with chemotherapy in patients with extensive stage small cell lung cancer. *Clin Cancer Res* **12**: 878–887.
64. Suzuki K and Matsubara H (2011). Recent advances in p53 research and cancer treatment. *BioMed Res Int* (article ID 978312, 7 pages).
65. Bourdon, JC (2007). p53 and its isoforms in cancer. *Br J Cancer* **97**: 277–282.
66. Alizadeh, AA, Eisen, MB, Davis, RE, Ma, C, Lossos, IS, Rosenwald, A *et al.* (2000). Distinct types of diffuse large B-cell lymphoma identified by gene expression profiling. *Nature* **403**: 503–511.
67. Golub, TR, Slonim, DK, Tamayo, P, Huard, C, Gaasenbeek, M, Mesirov, JP *et al.* (1999). Molecular classification of cancer: class discovery and class prediction by gene expression monitoring. *Science* **286**: 531–537.
68. Dörr, JR, Yu, Y, Milanovic, M, Beuster, G, Zasada, C, Däbritz, JH *et al.* (2013). Synthetic lethal metabolic targeting of cellular senescence in cancer therapy. *Nature* **501**: 421–425.
69. You, M, Zhu, G, Chen, T, Donovan, MJ and Tan, W (2015). Programmable and multiparameter DNA-based logic platform for cancer recognition and targeted therapy. *J Am Chem Soc* **137**: 667–674.
70. Morille, M, Passirani, C, Vonarbourg, A, Clavreul, A and Benoit, JP (2008). Progress in developing cationic vectors for non-viral systemic gene therapy against cancer. *Biomaterials* **29**: 3477–3496.
71. Xia, T, Kovochich, M, Liong, M, Meng, H, Kabehie, S, George, S *et al.* (2009). Polyethyleneimine coating enhances the cellular uptake of mesoporous silica nanoparticles and allows safe delivery of siRNA and DNA constructs. *ACS Nano* **3**: 3273–3286.
72. Kievit, FM, Veiseh, O, Bhattarai, N, Fang, C, Gunn, JW, Lee, D *et al.* (2009). PEI-PEG-chitosan copolymer coated iron oxide nanoparticles for safe gene delivery: synthesis, complexation, and transfection. *Adv Funct Mater* **19**: 2244–2251.
73. Zhu, L, Ma, J, Jia, N, Zhao, Y and Shen, H (2009). Chitosan-coated magnetic nanoparticles as carriers of 5-fluorouracil: preparation, characterization and cytotoxicity studies. *Colloids Surf B Biointerfaces* **68**: 1–6.
74. Jokerst, JV, Lobovkina, T, Zare, RN and Gambhir, SS (2011). Nanoparticle PEGylation for imaging and therapy. *Nanomedicine (Lond)* **6**: 715–728.
75. Yao, Y, He, Y, Guan, Q and Wu, Q (2014). A tetracycline expression system in combination with Sox9 for cartilage tissue engineering. *Biomaterials* **35**: 1898–1906.

Supplementary Information accompanies this paper on the Molecular Therapy–Nucleic Acids website (http://www.nature.com/mtna)